Alexandria Engineering Journal 105 (2024) 98–104

Contents lists available at ScienceDirect

Alexandria Engineering Journal

journal homepage: www.elsevier.com/locate/aej

Evaluation of the impact of PL/hBN and PL/B4C on the neutron leakage generated by the LINAC in the treatment room

Mehdi Hassanpour [a,*], Mohammad Rashed Iqbal Faruque [a,*], Marzieh Hassanpour [a], Mayeen Uddin Khandaker [b,c], K.S. Al-mugren [d]

[a] Space Science Centre (ANGKASA), Institute of Climate Change (IPI), Universiti Kebangsaan Malaysia, Malaysia
[b] Applied Physics and Radiation Technologies Group, CCDCU, School of Engineering and Technology, Sunway University, Bandar Sunway, Selangor 47500, Malaysia
[c] Faculty of Graduate Studies, Daffodil International University, Daffodil Smart City, Birulia, Savar, Dhaka 1216, Bangladesh
[d] Physics department, Science College, Princess Nourah bint Abdulrahman University, Riyadh, Saudi Arabia

ARTICLE INFO

Keywords:
Polyethylene/h-BN
Polyethylene/B4C
Neutron leakage
LINAC
MCNPX code
Neutron shielding

ABSTRACT

In this study, the maximal reduction of neutron leakage into the treatment room and bunker walls was evaluated by placing three stratified layers of PL/hBN and PL/B4C at distinct spatial coordinates within a medical linear accelerator facility. Simulations were conducted using the MCNPX code, focusing on "Photon flux per therapeutic X-ray dose" and "Neutron leakage and neutron density per therapeutic X-ray dose." The results indicated that adding PL/hBN and PL/B4C layers achieves the desired dose with a lower photon flux. The PL/hBN layer in a better proportion reduced flux compared to the PL/B4C layer. It was found that the PL/hBN layer can reduce neutron leakage and density in the air by up to 60.43 % and 50.08 %, respectively, while the PL/B4C layer achieved reductions of 44.32 % and 34.86 %. Additionally, reductions in neutron leakage and density within the bunker walls reached 95.61 % and 86.22 % with the PL/hBN shield, and up to 80.46 % and 70.59 % with the PL/B4C shield. These findings underscore the effectiveness of these layered neutron shielding measures in reducing neutron populations within the treatment room air and enhancing bunker protection.

1. Introduction

The examination of the inadvertent release of neutrons in the treatment room during radiotherapy for linear accelerators (Linac) is a crucial matter that has garnered considerable attention from researchers. Given that this subject has the potential to elucidate a meaningful connection between radiation physics and patient safety, it can be asserted that the study and establishment of an appropriate framework for advanced medical technology could greatly contribute to the well-being and radiation immunity of both patients and the medical personnel stationed at the healthcare facility.

1.1. The complexity of neutron radiation leakage

During the evolution of radiation therapy, remarkable advancements have been observed, with the emergence of Medical Linear Accelerators (Linac) being one of the pivotal milestones [9]. This is particularly notable due to its profound implications for precise dose delivery to the targeted area while minimizing radiation exposure to surrounding healthy tissues [18]. However, these advancements come with significant challenges, including the issue of neutron leakage [15].

The emergence of neutron radiation during the treatment with Medical Linear Accelerators (Linac) is fundamentally rooted in nuclear physics principles. When high-energy electrons within the MeV energy range collide with a specific target material characterized by a high atomic number, such as tungsten, they produce the desired spectrum of treatment photons and generate unwanted neutrons [12]. This leads to the release of high-energy neutrons into the treatment environment [13], resulting in unexpected consequences, as these high-penetrating neutrons can escape the confines of the accelerator vault and even penetrate the walls of the treatment room [14]. One concerning aspect in this regard is the leakage of neutrons with a wide energy spectrum, which complicates the preservation measures significantly. Therefore, the necessity of employing an appropriate method to mitigate the presence of unwanted neutrons to the greatest extent possible can be seen as a targeted approach that should be considered as a research imperative.

* Corresponding authors.
E-mail addresses: mhassanpour67@yahoo.com, p109951@siswa.ukm.edu.my (M. Hassanpour), rashed@ukm.edu.my (M.R.I. Faruque).

https://doi.org/10.1016/j.aej.2024.06.084
Received 19 March 2024; Received in revised form 6 June 2024; Accepted 26 June 2024
Available online 3 July 2024

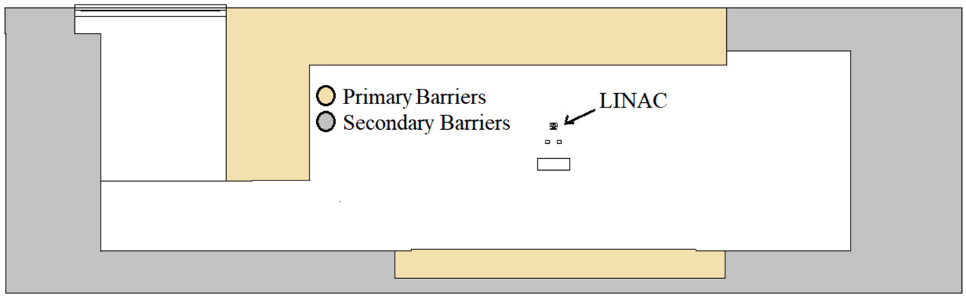

Fig. 1. A depiction of the interior layout within the treatment room, meticulously simulated using the MCNPX programming framework.

1.2. The intricacies of neutron interactions

Neutrons, devoid of electrical charge, predominantly engage with matter through nuclear forces, traversing materials with remarkable subtlety. The underlying physics of neutron interactions encompasses a tapestry of phenomena, encompassing elastic and inelastic scattering, neutron capture, and fission [11]. Each interaction mode possesses unique cross-sectional characteristics, energy dependencies, and material-specific behaviors. Consequently, the design of effective shielding materials requires a profound grasp of the intricate interplay of these processes, introducing a layer of perplexity that challenges even the most discerning physicists. Moreover, the dynamic interplay between neutron radiation and material properties introduces further complexity [1]. Neutron attenuation varies with material composition, density, and thickness, resulting in a multidimensional problem space where a multitude of factors converge to dictate shielding effectiveness. This complexity extends beyond theoretical considerations into the practical realm of treatment room design, where constraints such as spatial limitations and resource availability introduce real-world exigencies into the equation.

1.3. The Imperative for Innovative Shielding Strategies

Despite the inherent complexities associated with neutron interactions and energy spectra, the need to investigate and reduce neutron levels as much as possible necessitates an innovative approach to radiation protection. To address this challenge, cost-effective alternatives to experimental assessments have emerged in the form of Monte Carlo-based simulations [10]. These software tools possess high validation standards [17] and can serve as practical platforms for exploring various structures without limitations. The MCNPX code stands as one of the most significant Monte Carlo-based simulation codes, renowned as a pioneering tool across a wide spectrum of radiation applications, including its use in industries [4,7], Dairy and milk safety (Bahmani et al.,); radiography and radiotherapy [6], and various specialized applications such as nuclear detector development [3,8]. Therefore, this code has been employed as the primary tool in this research endeavor. This research aims to investigate the impact of polyethylene/hexagonal boron nitride (Pl/hBN) and polyethylene/ boron carbide (Pl/B4C) on reducing neutron leakage resulting from medical linear accelerators. Additionally, its effect on the quality of the photon spectrum produced by the Linac will also be examined. To achieve this goal, all input files for execution in the MCNPX code will be meticulously prepared. Based on

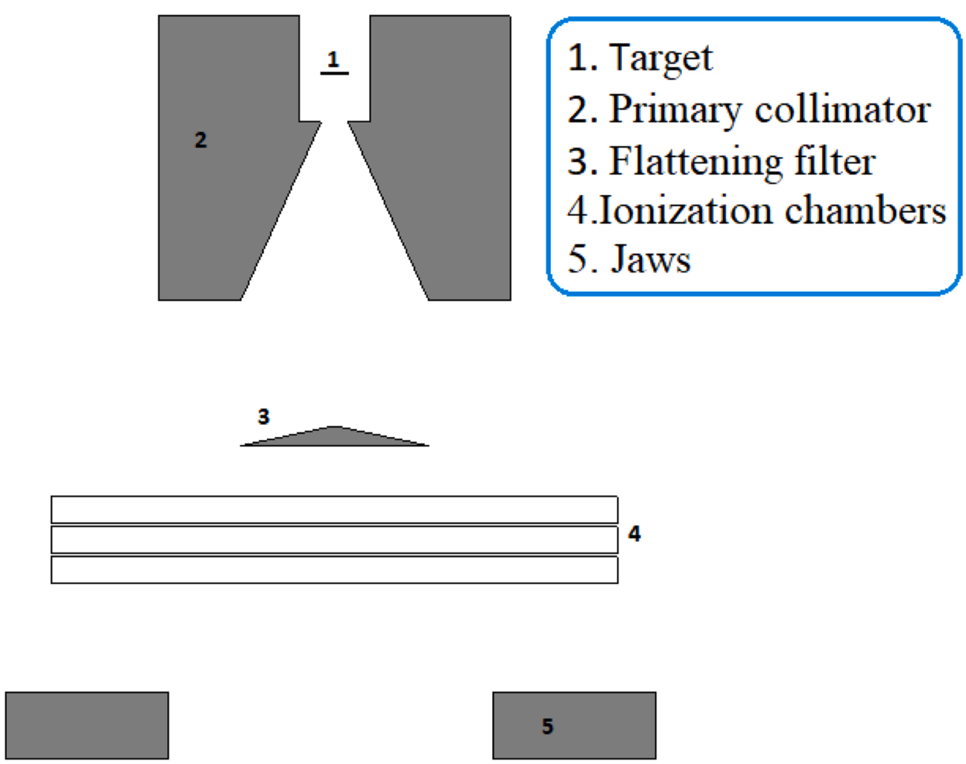

Fig. 2. The main components of Linac simulated in this research by MCNP code.

Table 1
The physical properties of Linac and treatment room key components [5], All the numbers mentioned in the table are in centimeters (cm).

Key components	Description	Dimension
Primary Collimator	The common area between the interior space of cylinder 1 with the exterior space of cylinder 2 and the truncated cone	Cylinder 1: H=9.6, R=2.5 Cylinder 2: H=3.6, R=0.5 Truncated Cone: H=6, R1=1.33, R2=0.2
Flattening filter	Truncated Cone	H=0.6675, R1=1.3335, R2=0.05
Tungsten target	Cylinder	H= 0.0635, R=0.2
Ionization chambers	Cylinder	First plate: H1=0.9, R1=4.01 Second plate: H2=0.9, R2=4.02 Third plate: H3=0.9, R3=4.03
Jaws	Rectangular cuboid	Z1 & Z2 Jaw: 20×7.5×5 X1 & X2 Jaw: 5×7.5×20
Primary barriers	Rectangular cuboids	High-Top Accelerator Walls (HTAW): 627×81× 582; 583×102×512 Low-Bottom Accelerator Walls: 400×60×512; 367×47×512 Maze or labyrinth Walls connected to HTAW: 492×119×412; 510×258×412; 111×70×412 Ceiling Walls: 482×602×147
Secondary barriers	Rectangular cuboids	The walls associated with various dimensions for shaping secondary barriers in rectangular cuboids have been considered.

the results of this research, which will be discussed in subsequent sections, manufacturers can utilize beneficial materials introduced as neutron shields in the accelerator head to prevent neutron emission into the treatment room. These results will be scientifically valuable for enhancing neutron shielding materials and can provide technical guidance for practical applications in accelerator facilities to improve safety protocols.

2. Materials and method

In the context of medical linear accelerator (Linac) therapy, the term "bunker" refers to a specific unit or location where linear accelerators and associated equipment are installed and operated. This facility is typically a room or building equipped with medical apparatus to carry out various stages of treatment using linear accelerators. The facility housing the accelerator, along with the accelerator itself, underwent comprehensive development and simulation. These processes were meticulously executed through the utilization of the MCNPX code, specifically tailored for the Siemens ONCOR linear accelerator, operating within the 18 MV beam spectrum, as depicted in Fig. 1.

For the design of a linear accelerator, various key components have been introduced in the MCNP code, including the collimator, flattening filter, and tungsten target (Fig. 2). The geometric specifications of each are provided in Table 1. This geometric structure is introduced in the MCNPX input file using the cell card and surface card.

A particle source of 18 MeV electron beam was defined in the input file that is directed perpendicularly onto the target to produce high-energy X-rays. The source-term details are defined by the SDEF card which defines the position, direction, and energy of the electron beam in the simulation. Additionally, material definitions in the Data card section of the input file are specified using ZAID, which is the product of the atomic number multiplied by one thousand and summed by the atomic

Table 2
The chemical composition of Linac and treatment room key components [16,2,5].

Elements	ZAID	Ordinary concrete (wt %)	Barite concrete (wt %)	Elements	ZAID	Ordinary concrete (wt %)	Barite concrete (wt %)
H	1001	0.0221	0.003585	Ca	20040	0.041526	0.048529
C	6000	0.002484	-	Ca	20042	0.000291	0.00034
O	8016	0.57493	-0.311622	Ca	20043	6.20E-05	7.30E-05
Na	11023	0.015208	-	Ca	20044	0.000974	0.001138
Mg	12024	0.000987	0.000932	Ca	20046	2.00E-06	2.00E-06
Mg	12025	0.00013	0.000123	Ca	20048	9.60E-05	0.000112
Mg	12026	0.000149	0.000141	Fe	26054	0.000367	0.002707
Al	13027	0.019953	0.004183	Fe	26056	0.005912	0.043643
Si	14030	0.010079	0.000346	Fe	26057	0.000138	0.001017
Si	14028	0.279871	0.009607	Fe	26058	1.90E-05	0.000138
Si	14029	0.014677	0.000504	Ba	56130	-	0.000465
S	16032	-	0.102191	Ba	56132	-	0.00045
S	16033	-	0.000832	Ba	56134	-	0.010935
S	16034	-	0.004811	Ba	56135	-	0.030014
S	16036	-	2.40E-05	Ba	56136	-	0.036001
K	19039	0.009336	-	Ba	56137	-	0.05188
K	19040	1.00E-06	-	Ba	56138	-	0.333656
K	19041	0.000708	-				
For PL/hBN & PL/B4C							
PL/hBN	Elements	ZAID	wt%	PL/B4C	Elements	ZAID	wt%
$\rho = 1.04$ g/cm^3	C	6012	0.72783727	$\rho = 0.972$ g/cm^3	C	6012	0.8435010
	H	1001	0.12216272		H	1001	0.1408464
	B	5010	0.06533037		B	5010	0.0156524
	N	7014	0.08466962				
For the primary collimator, flattening filter, tungsten, target, and jaws							
Elements	ZAID	wt%	Elements	ZAID	wt%		
W	74182	0.260586	W	74184	0.307531		
W	74183	0.142269	W	74186	0.289614		
Key components	Primary collimator	Flattening filter	Tungsten	Target	Jaws	Primary barriers	Secondary barriers
Density (gr/cm^3)	19.3	19.3	19.3	19.3	19.3	3.53	2.35

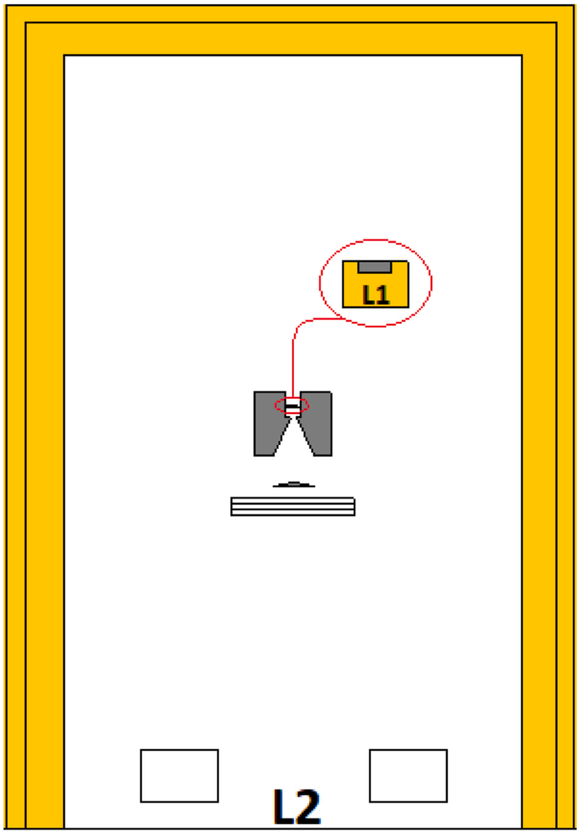

Fig. 3. Placement of Pl/hBN and Pl/B4C layers in the areas around the accelerator, 1) the first layer of the areas around the target, and 2) the second layer covering the entire accelerator.

mass number. The chemical composition of Linac key components and their element percentages have been inserted in Table 2.

The physical model defined for neutron production is as "phys:p 18 0 0 1 1". This physics model allows for (γ,n) and other photonuclear processes when photonuclear data tables are not available. MCNPX will mix and match, employing tables when available and physics models when tables are not. Cross-section data extracted from the ENDF/B-VI.6 library were used for particle production and transport. For photonuclear reactions, cross-section data from the ENDF/B-VII.0 library were utilized. To achieve a computational uncertainty below one percent, the number of particles for simulation was determined to be 10^8.

Continuing the simulation for the prevention of neutron leakage and its impact on the quality of the photon spectrums produced by the Linac, two layers filled with Pl/hBN and Pl/B4C were introduced in the input data file. The first layer, with a thickness of 2 millimeters, was considered cylindrical and placed around the target region. Additionally, to ensure direct interaction of the electron beam with the target, the top surface of the target was left uncovered by Pl/hBN and Pl/B4C in this setup.

The purpose of designing the first layer is to investigate its effect on the energy spectrum of photons generated by the Linac. Furthermore, the second and third cylindrical shape layers with different thicknesses of 5 and 7.5 centimeters, were placed around the entire accelerator equipment setup. It is worth noting that only the thickness of the bottom base of the cylinder, which is almost the passage location for photons, was considered to be 0.01 millimeters.

In Fig. 3, two surfaces, L1 and L2, have been considered for measuring the gamma spectrum using tally definitions. To achieve this, Tally F1 has been incorporated into the MCNPX input file. This tally is designed to detect the photon current rates from both surfaces, L1 and L2. To activate the gamma spectrum in the input file, auxiliary card E, along with card F, is invoked. The objective of defining the Pl/hBN and Pl/B4C layers was to maximize the reduction of neutrons in the treatment room. Therefore, to detect and track neutrons inside the treatment room air and the walls, two cards, "Population" and "Tracks entering," should be implemented in the code. These can be achieved by invoking Table 126 in the MCNPX output file. Therefore, the track entering and population results are obtained using the print table 126 command. It is noteworthy that the output of the code when using print table 126 includes various parameters such as collisions, flux, track weight, and track mean free path (mfp) in addition to track entering and population. Thus, it can be concluded that the type of tallies used in the input file does not affect the results of print table 126.

These measures will help monitor and analyze the behavior of neutrons in the treatment environment and assess the effectiveness of the Pl/hBN and Pl/B4C layers in reducing neutron leakage. An empirical repository serving as the veritable lynchpin for substantiation and integrity assurance of computational outcomes within the labyrinthine realm of Monte Carlo simulations.

In the domain of radiation therapy and nuclear physics simulations, the intrinsic constructs of "Tracks Entering" and "Population" manifest as pivotal variables, essential for comprehending particle kinetics within the confines of a treatment chamber. "Tracks Entering" constitutes an elemental metric, denoting the numerical tally of particles, in this research neutrons, traversing distinct spatial sectors within the treatment chamber's geometric configuration. These particles, upon their inception, embark upon intricate trajectories, ushering in consequential nuclear interactions pivotal for modeling radiation therapy and nuclear physics phenomena. In contradistinction, "Population" represents a more comprehensive numerical abstraction, encompassing the comprehensive consortium of neutrons distributed throughout voluminous regions within the treatment enclosure. This aggregation transcends the purview of the initial assemblage signified by "Tracks Entering," as it encompasses secondary neutrons resulting from subsequent nuclear reactions and interactions.

2.1. Backscattering phenomena

An intriguing facet of particle kinetics meriting discerning scrutiny is the phenomenon of backscattering. This phenomenon unfolds as particles undergo directional perturbations after interacting with constituent materials of the treatment chamber, ultimately retracing their trajectories in an antithetical vectorial orientation. The quantification of this phenomenon is predicated upon a rudimentary arithmetic operation—the subtrahend of "Tracks Entering" from the overarching "Population." This numeric deduction confers profound insights into the amplitude of particles deviating from their original trajectories, thereby augmenting the comprehension of radiation distribution dynamics.

2.2. Dosimetric characteristics of photon beam

To calculate the dose from photon radiation and analyse it, a water phantom with dimensions of 40×40×40 cm^3 was defined in the input file with a source-to-surface distance (SSD) of 100 cm. The thickness of the phantom was divided into forty equal parts, and the dose received at each thickness was determined using Mesh tally type 1.

3. Results and discussion

3.1. Investigating the effect of Pl/hBN and Pl/B4C layers defined in the areas around Linac on the energy spectrum of photons produced in the accelerator head

Initially, the dose rate per mA (Sv/mA.s) was evaluated across three different thicknesses of the phantom. These three thicknesses include the surface of the phantom, a depth of 10 cm from the phantom surface, and the thickness at which the dose is at its maximum. The results are

Table 3
Dose rate per mA (Sv/mA.s) at three thicknesses of the phantom: 0 cm, 2 cm, and 10 cm.

Phantom Depth = 0 (cm)			
Materials	Original	Pl/hBN	Pl/B4C
Dose per particle (Sv/SP)	5.58E-16	6.07E-16	5.85E-16
Dose rate per mA (Sv/mA.s)	3.49	3.79	3.66
Phantom Depth = 2 (cm) (where the dose is Maximum)			
Materials	Original	Pl/hBN	Pl/B4C
Dose per particle (Sv/SP)	5.63E-16	6.14E-16	5.87E-16
Dose rate per mA (Sv/mA.s)	3.52	3.83	3.67
Phantom Depth = 10 (cm)			
Materials	Original	Pl/hBN	Pl/B4C
Dose per particle (Sv/SP)	4.73E-16	5.50E-16	5.18E-16
Dose rate per mA (Sv/mA.s)	2.95	3.43	3.24

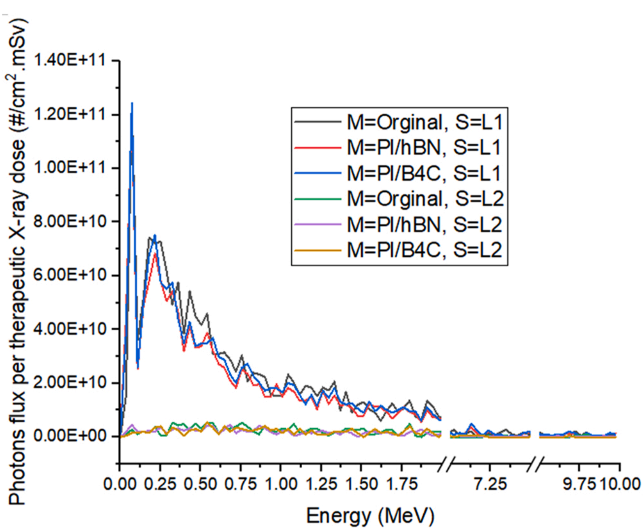

Fig. 4. The photons flux per therapeutic X-ray dose (#/cm^2.mSv). Presented in two scenarios: one in the presence of the Pl/hBN and Pl/B4C layers surrounding the target and another in its absence.

presented in Table 3. It is noteworthy that to convert the mesh tally output to dose rate per mA, the results were multiplied by 6.25E+15. This conversion factor was derived using Eq. 1.

$$n = \frac{i \quad (A) \quad \times t(s)}{e \quad (C)} \tag{1}$$

where n is the number of electrons in the accelerator current i in amperes (A), t is time in seconds (s), and e is the electric charge in coulombs (C). For an electric current of 1 mA and an irradiation time of 1 s, n equals 6.25E+15. The unit sievert (Sv) is used instead of gray (Gy) because the radiation weighting factor for photons is one.

The results in Table 3 demonstrate that the Dose rate per mA for the Pl/hBN shield is higher than that for Pl/B4C and the original unshielded condition in the phantom under deposition. In Fig. 3, two distinct levels, denoted L1 and L2, as observable, have been designated for the photon spectrum detection. L1 is positioned precisely following the tungsten target, while L2 is situated beyond the Jaws apparatus. The resultant photon spectrum, both with and without the presence of Pl/hBN and Pl/B4C layers, has been obtained by an F1 tally along with auxiliary card E.

Table 4
The IPOP percentage by considering various configurations of Pl/hBN and Pl/B4C layers within the bunker.

Material (M)	For Pl/hBN	For Pl/B4C
	IPOP (%)	
S=L1	10.49554196	5.037691734
S=L2	17.51831371	15.20185865

Table 5
Population and track entering per therapeutic X-ray dose (#/mSv).

Track entering or neutron leakage per therapeutic X-ray dose (#/mSv)				
Material	ORIGINAL	Pl/hBN (First Layer)	Pl/hBN (Second Layer)	Pl/hBN (Third Layer)
AIR	7.13E+11	5.18E+11	3.23E+11	2.82E+11
Bunker's Barriers	2.81E+11	2.28E+11	4.03E+10	1.23E+10
Track entering per therapeutic X-ray dose (#/mSv)				
Material	ORIGINAL	Pl/B4C (First Layer)	Pl/B4C (Second Layer)	Pl/B4C (Third Layer)
AIR	7.13E+11	5.82E+11	4.21E+11	3.97E+11
Bunker's Barriers	2.81E+11	2.34E+11	9.05E+10	5.48E+10
Population per therapeutic X-ray dose (#/mSv)				
Material	ORIGINAL	Pl/hBN (First Layer)	Pl/hBN (Second Layer)	Pl/hBN (Third Layer)
AIR	3.57E+11	2.54E+11	1.94E+11	1.78E+11
Bunker's Barriers	3.38E+11	2.81E+11	8.01E+10	4.65E+10
Population per therapeutic X-ray dose (#/mSv)				
Material	ORIGINAL	Pl/B4C (First Layer)	Pl/B4C (Second Layer)	Pl/B4C (Third Layer)
AIR	3.57E+11	2.94E+11	2.45E+11	2.32E+11
Bunker's Barriers	3.38E+11	2.98E+11	1.44E+11	9.93E+10

Finally, to normalize the results in terms of therapeutic X-ray dose, the obtained values were divided by the remaining dose in the 10 cm thickness of the water phantom. The results are presented in Fig. 4 in units of #/cm^2.mSv. This graph illustrates the photon fluence that can result in depositing one milli-sievert dose in the 10 cm thickness of the water phantom. The symbols "M=Orginal, S=L1", "M= Pl/hBN, S=L1", "M=Pl/B4C, S=L1", "M=Orginal, S=L2", "M= Pl/hBN, S=L2", "M=Pl/B4C, S=L2" correspond, respectively, to the photons flux per therapeutic X-ray dose in the material type (M) and the related surface (L1 & L2).

For better clarity in Fig. 4, the results obtained for energies 2 MeV and above have been broken at two breakpoints. Fig. 4 results indicate that to maintain a 1 mSv dose in the 10 cm depth of the water phantom, the photon fluence exiting the accelerator head is higher for the normal condition compared to when Pl/hBN and Pl/B4C shields are considered. As a result, the addition of Pl/hBN and Pl/B4C layers redistributes the energy distribution of outgoing photon fluence so that with lower fluence, it can deposit a 1 mSv dose in the 10 cm depth of the deposit.

Permit me to delve deeper into a more precise exploration as we endeavor to define the concept of "Improvement Percentage of Output Photon Spectrum (IPOP)," which may be expressed as Eq. 2.

$$IPOP = \frac{\sum FDCC\ with\ Shield \quad (per\ mSv) \quad - \quad \sum FDCC\ without\ Shield \quad (per\ mSv)}{\sum FDCC\ without\ Shield \quad (per\ mSv)} \times 100 \tag{2}$$

where FDCC is the abbreviation of the flux-dose conversion coefficient. The IPOP results for Pl/hBN and Pl/B4C shields at two levels, L1 and L2, are presented in Table 4.

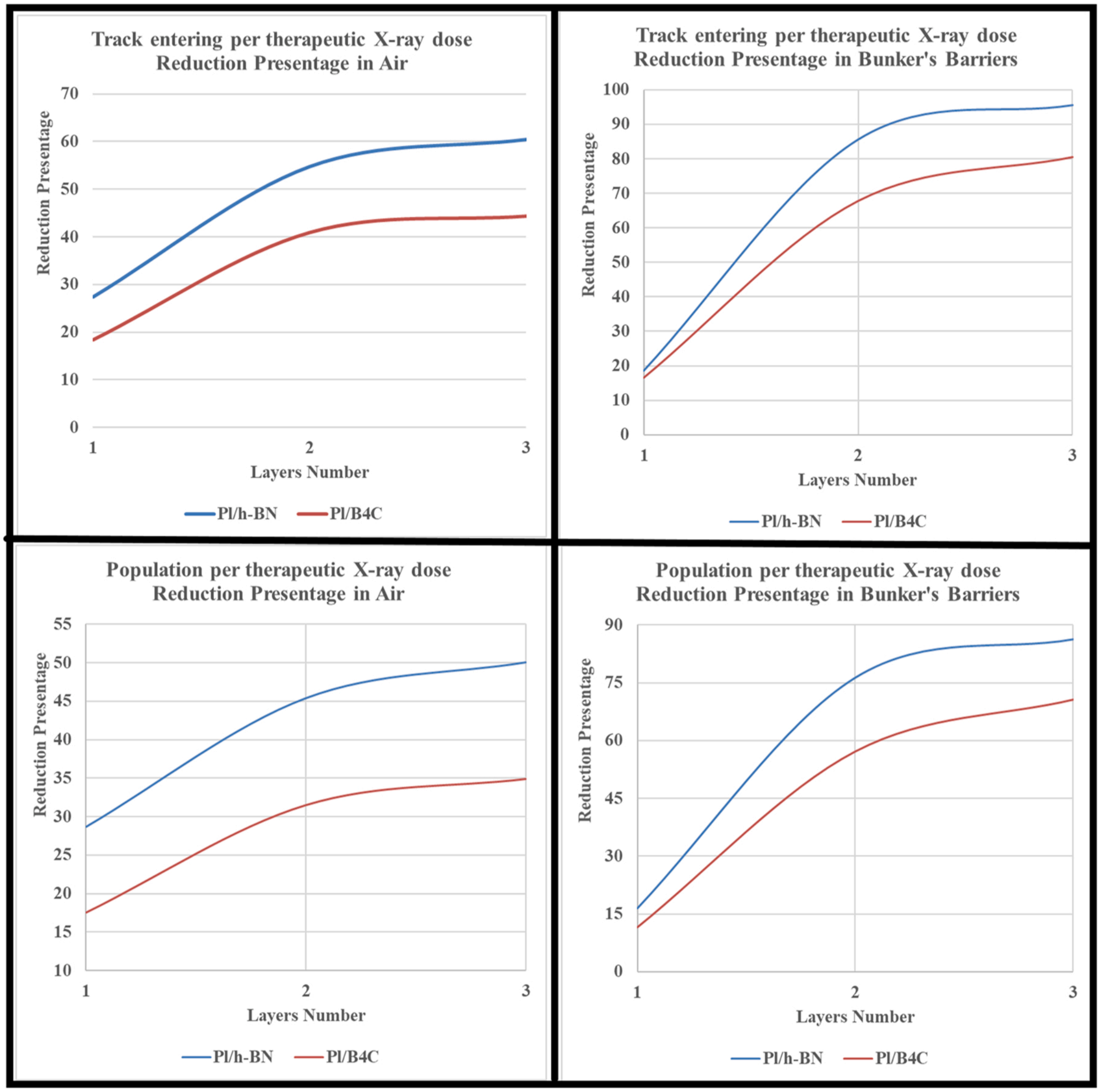

Fig. 5. Population and track entering per therapeutic X-ray dose reduction percentage in the bunker's barriers and air.

Based on the results in this table, it can be inferred that the Pl/hBN layer leads to a greater reduction in fluence compared to the Pl/B4C layer in delivering a specific dose to the patient at both levels, L1 and L2. Overall, achieving the desired dose with a reduced photon flux in radiation therapy can be beneficial. This approach can lead to reduced scatter radiation, thereby decreasing exposure to surrounding healthy tissues and organs, which in turn can reduce side effects and complications. Additionally, lowering the photon flux can improve precision in targeting the tumor, preventing radiation "spill" into adjacent healthy tissues. From a technical standpoint, this strategy can reduce wear and tear on linear accelerator machines and increase energy efficiency. Reduced photon flux can also potentially shorten treatment sessions, increasing patient comfort, and providing wider safety margins, reducing the risk of accidental overexposure.

3.2. Investigating the reduction of neutron leakage in the bunker walls and the internal atmosphere

The population and tracks entering or neutron leakage were calculated after the collision of 18 MeV electrons with the accelerator. The population and tracks entering obtained from the code are divided by the number of electron particles (SP) and the dose at a depth of 10 cm per particle from the source. The result is termed Population or track entering per therapeutic X-ray dose, reported in units of #/mSv.

The results are visible in Table 5. It is worth mentioning that each of these two parameters was considered for each component of the bunker individually, and their cumulative values have been reported.

Table 5 presents the neutron leakage and neutron density (population) in the air and walls of the treatment room when the received dose at a depth of 10 centimeters is equivalent to 1 millisievert. The data is shown for various layers of two materials: Pl/B4C and Pl/hBN. As the number of layers increases, these quantities decrease compared to the original unshielded state. The material Pl/hBN exhibits the best performance, with lower neutron leakage and population across all regions compared to both Pl/B4C and the unshielded state. By defining the percentage reduction in leakage and population according to the IPOP formula, the aforementioned results are illustrated in Fig. 5. The results indicate that both the track entering and population percentage reductions are higher for the Pl/hBN layers compared to the Pl/B4C layers.

It is important to note that the "track entering" refers to the neutron leakage from the accelerator head into the air and walls of the treatment room. On the other hand, "population" denotes the number of neutrons present in each part of the treatment room, which may differ from the neutron leakage. This discrepancy arises because the leaking neutrons can be absorbed by the walls and air, or additional neutrons may be generated as a result of collisions.

4. Conclusion

In this study, the impact of placing three layers of PL/h-BN and PL/B4C at different spatial coordinates within the medical linear accelerator on the maximal reduction of neutron leakage into the treatment room's interior atmosphere and bunker walls was evaluated. Initially, the photon spectrum resulting from the original target without shielding and with PL/B4C and PL/hBN shields was obtained using the MCNPX code with the F1 tally and relevant auxiliary cards. This spectrum was then converted to photon flux per therapeutic X-ray dose by dividing the values by the dose deposited at a depth of 10 cm in a water phantom. The results indicate that adding Pl/hBN and Pl/B4C layers can achieve the equivalent dose of the original state in the phantom by reducing the outgoing photon flux. Notably, the Pl/hBN layer results in a greater reduction in flux compared to the Pl/B4C layer when delivering a specified dose to the patient.

Next, investigations were simulated using the MCNPX code for two parameters: neutron "Tracks Entering" and neutron "Population." After extracting the results for these two parameters, the data was standardized to report population or track entering per therapeutic X-ray dose. This was done by dividing the results by the number of source particles (SP) and the dose at a depth of 10 cm in the phantom per single source particle. The findings show that, for a fixed photon dose of 1 mSv in the water phantom, adding Pl/hBN and Pl/B4C layers can reduce neutron leakage and neutron density in the air by up to 60.43 % and 50.08 % for Pl/hBN, and up to 44.32 % and 34.86 % for PL/B4C, respectively. Additionally, the reduction in neutron leakage and neutron density within the bunker walls with the Pl/hBN shield can reach up to 95.61 % and 86.22 %, respectively. For the PL/B4C shield, these reductions can be up to 80.46 % and 70.59 %, respectively.

On the other hand, excellent compatibility between h-BN and polymers, such as polyethylene, can make mixing and dispersion easier and improve the production process. Moreover, h-BN's layered structure facilitates the creation of homogeneous composites. On the other hand, B4C is harder and more abrasive, which might make it more difficult to disseminate uniformly in a polymer matrix, complicating the production process.

In conclusion, both shields, Pl/hBN and Pl/B4C, proposed in this study can enhance the quality of radiotherapy with Linac. Moreover, they can significantly reduce neutron presence in the treatment room air and bunker walls, thereby improving radiation safety for both personnel and patients.

CRediT authorship contribution statement

Marzieh Hassanpour: Writing – original draft, Visualization, Validation, Software, Methodology, Investigation, Formal analysis, Data curation, Conceptualization. **Mohammad Rashed Iqbal Faruque:** Writing – review & editing, Validation, Supervision, Resources, Project administration, Methodology, Funding acquisition. **Mehdi Hassanpour:** Writing – review & editing, Writing – original draft, Visualization, Validation, Software, Methodology, Investigation, Formal analysis, Data curation, Conceptualization. **K. S. Al-mugren:** Writing – review & editing, Resources, Investigation, Funding acquisition. **Mayeen Uddin Khandaker:** Writing – review & editing, Validation, Supervision, Resources.

Declaration of Generative AI and AI-assisted technologies in the writing process

During the preparation of this work, the authors used ChatGPT in order to edit the writing of the written manuscript. After using this tool/service, the authors reviewed and edited the content as needed and takes full responsibility for the content of the publication.

Declaration of Competing Interest

The authors declare that they have no known competing financial interests or personal relationships that could have appeared to influence the work reported in this paper.

Acknowledgments

This research was funded by Fundamental Research Grant Scheme (FRGS), MOE, Malaysia, Code: FRGS/1/2022/TK07/UKM/02/22. Moreover, this research acknowledges the Princess Nourah bint Abdulrahman University Researchers Supporting Project number (PNURSP2024R10), Princess Nourah bint Abdulrahman University, Riyadh, Saudi Arabia.

References

[1] R.C. Baumann, Soft errors in advanced semiconductor devices-part I: the three radiation sources, IEEE Trans. Device Mater. Reliab. 1 (1) (2001) 17–22.
[2] C. Harrison, E. Burgett, N. Hertel, E. Grulke, Polyethylene/Boron Composites For Radiation Shielding Applications (January), in: In AIP Conference Proceedings, Vol. 969, American Institute of Physics, 2008, pp. 484–491 (January).
[3] M. Hassanpour, M. Rezaie, M. Hassanpour, M.R.I. Faruque, M.U. Khandaker, Monte Carlo simulation of spallation fragments cross-sections and yield for proton beam interaction with 222Rn, Alex. Eng. J. 87 (2024) 652–661.
[4] M. Hassanpour, M. Hassanpour, M.U. Khandaker, M.R.I. Faruque, B. Alshahrani, H. Osman, An alternative method for calculation of half-value layers without the knowledge of attenuation coefficient, Appl. Radiat. Isot. (2023) 110910.
[5] L. IsolanVerifica radioprotezionistica con tecniche Monte Carlo del bunker per radioterapia dell'ASMN-IRCCS di Reggio Emilia.
[6] M.U. Khandaker, M. Hassanpour, S. Khezripour, M.R. Rezaei, A. Bazghandi, M. Hassanpour, M.R.I. Faruque, D.A. Bradley, Investigation of the effect of 131I on blood parameters for thyroid cancer treatment, Radiat. Phys. Chem. 208 (2023) 110897.
[7] S. Khezripour, M. Rezaie, M. Hassanpour, M. Hassanpour, M. Rashed Iqbal Faruque, M. Uddin Khandaker, Investigating the hard X-ray production via proton spallation on different materials to detect elements, PloS One 18 (8) (2023) 0288287.
[8] S. Khezripour, A. Negarestani, M.R. Rezaie, Investigating the response of Micromegas detector to low-energy neutrons using Monte Carlo simulation, J. Instrum. 12 (08) (2017) p.4P08007.
[9] V. Kong, V.N. Hansen, S. Hafeez, Image-guided adaptive radiotherapy for bladder cancer, Clin. Oncol. 33 (6) (2021) 350–368.
[10] H. Marzieh, S. Faghihi, S. Khezripour, M. Rezaie, P. Dehghanipour, M.R.I. Faruque, M.U. Khandaker, Introduction of graphene/h-BN metamaterial as neutron radiation shielding by implementing Monte Carlo simulation, Materials 15 (19) (2022) 6667.
[11] M.R. Mumpower, P. Talou, R. Vogt, Impact on Science and Technology. In Nuclear Fission: Theories, Experiments and Applications, Springer International Publishing, Cham, 2022, pp. 401–464.
[12] A. Naseri, A. Mesbahi, A review on photoneutrons characteristics in radiation therapy with high-energy photon beams, Rep. Pract. Oncol. Radiother. 15 (5) (2010) 138–144.
[13] U. Oflaz, İ.H. Sarpün, H. Özdoğan, Investigation of level density and Gama strength function for photoneutron reaction in medical linacs in Beamline, Appl. Radiat. Isot. (2022) 110286.
[14] C. Ongaro, A. Zanini, U. Nastasi, J. Ródenas, G. Ottaviano, C. Manfredotti, Analysis of photoneutron spectra produced in medical accelerators, Phys. Med. Biol. 45 (12) (2000) L55.
[15] I.A. Ouaggou, D. Bakari, A. Rrhioua, M. Zerfaoui, Y. Oulhouq, M. Talbi, M. Benmessaoud, Evaluation of ambient dose equivalent for photoneutrons around linear accelerator and their radioprotection quantities, Radiat. Phys. Chem. (2023) 111096.
[16] Y. Shang, G. Yang, F. Su, Y. Feng, Y. Ji, D. Liu, R. Yin, C. Liu, C. Shen, Multilayer polyethylene/hexagonal boron nitride composites showing high neutron shielding efficiency and thermal conductivity, Compos. Commun. 19 (2020) 147–153.
[17] B. Van, Y.K. Dewaraja, J.T. Niedbala, G. Rosebush, M. Kazmierski, D. Hubers, J. K. Mikell, S.J. Wilderman, Experimental validation of Monte Carlo dosimetry for therapeutic beta emitters with radiochromic film in a 3D-printed phantom, Med. Phys. 50 (1) (2023) 540–556.
[18] H.R. Vega-Carrillo, T.G. Soto-Bernal, Neutrons produced in a 12 MV LINAC working in electron mode, Radiat. Phys. Chem. 208 (2023) 110905.